Peptide Inhibitors of Bacterial Protein Synthesis with Broad Spectrum and SbmA-Independent Bactericidal Activity against Clinical Pathogens

Mario Mardirossian, Riccardo Sola, Bertrand Beckert, Erica Valencic, Dominic W. P. Collis, Jure Borišek, Federica Armas, Adriana Di Stasi, Jan Buchmann, Egor A. Syroegin, Yury S. Polikanov, Alessandra Magistrato, Kai Hilpert, Daniel N. Wilson, and Marco Scocchi*

ABSTRACT: Proline-rich antimicrobial peptides (PrAMPs) are promising lead compounds for developing new antimicrobials; however, their narrow spectrum of action is limiting. PrAMPs kill bacteria binding to their ribosomes and inhibiting protein synthesis. In this study, 133 derivatives of the PrAMP Bac7(1−16) were synthesized to identify the crucial residues for ribosome inactivation and antimicrobial activity. Then, five new Bac7(1−16) derivatives were conceived and characterized by antibacterial and membrane permeabilization assays, X-ray crystallography, and molecular dynamics simulations. Some derivatives displayed broad spectrum activity, encompassing *Escherichia coli*, *Klebsiella pneumoniae*, *Acinetobacter baumanii*, *Pseudomonas aeruginosa*, and *Staphylococcus aureus*. Two peptides out of five acquired a weak membrane-perturbing activity while maintaining the ability to inhibit protein synthesis. These derivatives became independent of the SbmA transporter, commonly used by native PrAMPs, suggesting that they obtained a novel route to enter bacterial cells. PrAMP-derived compounds could become new-generation antimicrobials to combat antibiotic-resistant pathogens.

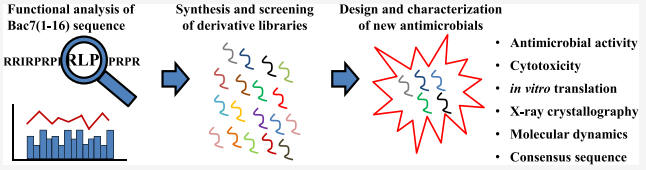

INTRODUCTION

The search for new antimicrobial agents is propelled by the continuous emergence of antibiotic-resistant pathogens.[1] In recent years, there has been increasing interest in testing antimicrobial peptides (AMPs) as lead compounds for the development of new antibiotics.[2] Proline-rich AMPs (PrAMPs) are particularly promising as they combine potent antimicrobial activity with low toxicity toward eukaryotic cells,[3] a feature owing to their nonlytic mode of action.[4] PrAMPs do not permeabilize the bacterial membranes,[4] but rather they enter the cells of several Gram-negative species (e.g., *Enterobacteriaceae*) by active transport using predominantly the bacterial inner membrane transporter SbmA.[3,5−7] Once inside the bacterial cell, PrAMPs kill bacteria by binding to their ribosomes and inhibiting protein synthesis.[8−10] Two distinct mechanisms of action have so far been described in molecular details for different PrAMPs: (i) type I PrAMPs allow initiation of protein synthesis but prevent the transition into the elongation phase by impeding the accommodation of the first aminoacyl-tRNA,[11−16] whereas (ii) type II PrAMPs allow initiation and elongation of protein synthesis but interfere with translation termination by trapping the release factors on the ribosome.[17,18] Interestingly, inhibition of bacterial protein synthesis is a feature shared by PrAMPs present in phylogenetically distinct organisms, such as insects (apidaecins and oncocins) and mammals (Bac7 and Bac5 derivatives as well as Tur1A), most probably as a result of convergent evolution.[3] The distinctive mode of transport of PrAMPs into bacterial cells using the bacterial membrane protein SbmA makes PrAMP activity strongly dependent on the presence of this transporter, thus limiting their spectrum of activity mainly to those pathogens that express SbmA.[3]

During the recent years, some mammalian and insect PrAMPs were subjected to systematic sequence and length modifications with the aim of improving their antimicrobial potential, their spectrum activity, as well as reducing the cost of manufacturing.[19−24] Peptide libraries designed on the insect-derived apidaecin[19,25] and oncocin[20,26] were synthesized by SPOT synthesis and tested for their antimicrobial effect. Some of these variants were identified with improved antimicrobial activity against pathogens, such as *Pseudomonas aeruginosa*, *Staphylococcus aureus*, and *Escherichia coli*. A similar approach was applied to a derivative of the mammalian PrAMP Bac5(1−17), resulting in peptides with improved antimicrobial effect against *E. coli*, *Klebsiella pneumoniae*, and *Acinetobacter*

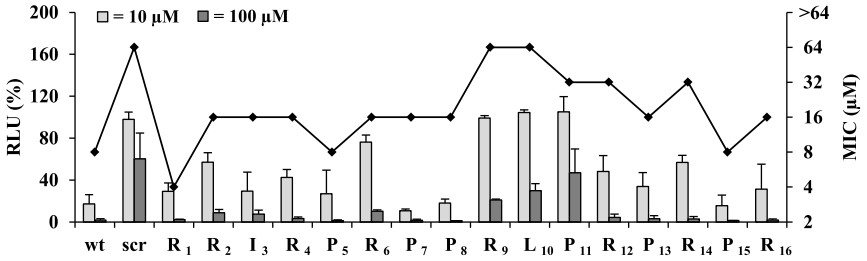

Figure 1. Luminescence after *in vitro* transcription/translation using *E. coli* lysates (histograms) and MIC values on *E. coli* cells (black line) in the presence of Bac7(1−16) alanine-substituted variants. The peptide sequence is displayed on the *x*-axis. The values above each residue refer to the peptide carrying the alanine substitution in that position. Unmodified (wt) and scrambled (scr) peptides were used as controls. Transcription/translation reactions (left *y*-axis) were performed in the presence of 10 μM (light gray) and 100 μM (dark gray) peptides. Luminescence of the translated luciferase was normalized using the untreated controls (RLU %). Error bars indicate the standard deviation calculated on the mean of at least two independent experiments. MIC values (right *y*-axis and black line) against *E. coli* BW25113 are the median calculated on at least three independent experiments.

Table 1. MIC Values (μM) against *E. coli* BW25113 of the Wild-Type Bac7(1−16) Compared with Scrambled and Substituted Variants[a]

Bac7 (1-16)[b]	MIC (µM)									
	wt[c]	scr[d]	G	A[e]	S	P	R	E	F	W
R_1	8	64	8	4	16	8	-	64	4	2
R_2			16	16	16	64	-	64	16	8
I_3			16	16	16	16	8	64	16	4
R_4			16	16	32	16	-	>64	16	8
P_5			8	8	16	-	8	32	8	4
R_6			32	16	32	32	-	>64	16	8
P_7			16	16	16	-	8	32	8	4
P_8			16	16	16	-	16	64	16	4
R_9			64	64	32	16	-	>64	16	4
L_{10}			64	64	32	64	32	>64	32	16
P_{11}			32	32	32	-	16	64	32	8
R_{12}			32	32	16	32	-	>64	16	8
P_{13}			16	16	16	-	8	64	8	2
R_{14}			32	32	32	32	-	64	8	4
P_{15}			16	8	16	-	16	32	8	4
R_{16}			16	16	16	32	-	64	8	8

[a]Substitutions improving antimicrobial activity compared to the native Bac5(1−17) are highlighted with gray shading. [b]Bac7(1−16) sequence and position numbers. [c]Bac7(1−16) wild-type. [d]Bac7(1−16) scrambled: IRPLPPRRPRRPRRRP. [e]For comparison the Ala-scan MIC values from Figure 1 are also included in this table. Results are reported as median of at least three independent experiments ($n \geq 3$).

baumannii.[22] N-terminal fragments of the native mammalian PrAMPs Bac7[27] are among the best characterized mammalian PrAMPs. However, their systematic modification to identify new derivatives with improved antimicrobial properties is still embryonic[21,28] and deserves further and broader efforts.

In this work, we systematically modified Bac7(1−16) to identify the amino acid residues that are essential for the ribosome binding and antimicrobial activity. These data were then used to direct the design of novel derivatives with increasing antimicrobial properties. Five derivatives were conceived and analyzed for their activity and mechanism of action. X-ray crystallography and molecular dynamics (MD) simulations[29,30] were then employed to obtain structural insights into the binding mode of these peptides with their target. Our results reveal that residues Arg_9−Arg_{12} of Bac7(1−16) are crucial for the inhibition of bacterial growth and protein synthesis. The introduction of Arg and Trp residues in specific positions of the peptide's sequence modified the mode of some derivatives to enter bacteria and promoted their antimicrobial activity against a broadened spectrum of bacterial pathogens. These data provide new insights for the rational design of more potent antimicrobial drugs, which are urgently needed to fight the growing tide of antibiotic-resistant bacterial infections.

RESULTS

Identification of Bac7(1−16) Residues Essential for the Inhibition of Protein Synthesis. To identify the residues of Bac7(1−16) essential for antimicrobial activity, a library of 16 peptides was prepared where each residue was individually replaced by alanine. The antimicrobial activity and the protein synthesis-inhibiting activity of the modified peptides were assessed by determination of the minimum inhibitory concentration (MIC) as well as using an *in vitro* transcription/translation assay, respectively (Figure 1). The substitution of any residue in the $_9RLP_{11}$ portion of the

Table 2. Antimicrobial Activity in the Absence or Presence of Serum and Cytotoxicity of Purified Bac7(1−16) Derivatives[a]

B7-code	sequence	MIC on *E. coli* (μM)			CytoTox[d] (μM)
		BW25113	ATCC 25922	ATCC 25922 + ser[c]	
wt[b]	RRIRPRPPRLPRPRPR	2	1	1	>64
001	WRIRPRPPRLPRPRPR	1	1	1	>64
002	RRIRPRPPRLPRPRWR	1	1	1.5	>64
003	WRIRPRPPRLPRWRPR	2	1.5	2	>64
004	WRIRRPPRLPRPRWR	1	1	6	>64
005	WRIRRRWPRLPRPRWR	2	1	3	>64

[a]Results are the median of at least three independent experiments ($n = 3$). [b]wt = wild-type Bac7(1−16). [c]ser = 10% (v/v) human serum in full MH medium. [d]CytoTox = p-value ≤ 0.05, Student's t-test, peptide-treated MEC-1 cells vs untreated control.

Bac7(1−16) dramatically reduced its potential to inhibit both bacterial protein synthesis and the growth of *E. coli* cells. Amino acid substitutions in other regions were better tolerated, and the replacement of Arg1 with Ala (R1A) was even a beneficial change, improving the antimicrobial activity of the peptide. The similar trend between the MICs and the inhibition of the transcription/translation suggested that changes in antimicrobial activity of the peptide variants were mainly due to a corresponding change in the inhibitory activity on protein synthesis.

Activity of Bac7(1−16) Variants Bearing Diverse Amino Acid Substitutions. To identify novel Bac7(1−16) derivatives with improved antimicrobial activity with respect to the original Bac7(1−16) peptide, a new peptide library (114 members) was prepared by SPOT-synthesis. Each Bac7(1−16) residue was substituted with glycine, alanine, or serine (absent, short nonpolar, or polar side chain, respectively), proline (secondary structure-disrupting residue), arginine or glutamic acid (long basic or acidic side chain), and phenylalanine or tryptophan (bulky aromatic side chain). All members of this peptide library were then tested by MIC assays in full Müller−Hinton medium on *E. coli* BW25113 (Table 1). In 61.6% of the substitutions, only a small change in the MIC values was measured (twofold change compared to wild type) (Table S1). R1W and P13W substitutions, representing 1.8% of all the peptides, showed a fourfold improvement in the MIC values (MIC = 2 μM). In 31.1% of the substitutions, the MIC values dropped to 4−8-fold and 4.4% showed no activity at the highest concentration measured (64 μM). The positions R9, L10, P11, R12, and R14 showed the least amount of tolerance to substitutions, with most of the substitutions showing a medium to strong decrease in antimicrobial activity (Table S1). Most substitutions with Gly (G), Ala (A), Ser (S), and Pro (P) led to a decreased antibacterial effect. The substitution with Glu (E) was always adverse, leading to inactivation of the peptide regardless of the position (MICs 32 microM to >64 μM), similar to the effect of the scrambled peptide used as a control (Table 1). This result was not surprising given that the binding of Bac7(1−16) with the ribosome involves several arginines that form hydrogen bonds with nucleotides of the 23S rRNA as well as electrostatic interactions with its phosphate groups.[11] In contrast, amino acid substitutions with Arg (R), Phe (F), or Trp (W) were well tolerated, resulting in unchanged or improved antimicrobial activity (Table 1). This result was consistent with the general binding mode proposed for PrAMPs on the ribosome where the side chains of arginines and aromatic residues establish multiple stacking interactions with the rRNA.[11]

Antimicrobial Activity and Biocompatibility of Mono- and Multisubstituted Bac7(1−16) Derivatives. Introduction of different Arg and Trp residues, which singularly often increased antimicrobial activity of Bac7(1−16) (Table 1), was combined to design new Bac7(1−16) multisubstituted derivatives. Two positions within the Bac7(1−16) peptide, namely, R1 and P13, when substituted by (W) led to the best activity improvements (2 μM, Table 1). We combined these modifications to produce the di-substituted Bac7(1−16) derivative B7-003 (Table 2). We then tried different substitutions to generate the tri- and tetra-substituted Bac7(1−16) derivatives B7-004 and B7-005 (Table 2). These derivatives displayed R, W, and W residues at positions P5, P7, and P15, respectively, where the substitution with other amino acids (namely, G, A, R, F for P5; R, F for P7; and A, F for P15) was also well-tolerated. These five derivatives were synthesized on resin by solid-phase and highly purified (purity ≥95%) together with the wild-type Bac7(1−16) as a control. B7-001 and B7-002, which were the most active single substituted peptides bearing the substitution as far as possible from the critical R_9−P_{11} residues, were also synthesized (Table 2).

All these highly purified peptides displayed an MIC of 1−2 μM against *E. coli* BW25113 and *E. coli* ATCC 25922 (Table 2). None of the multisubstituted peptides possessed a higher antimicrobial activity than the wild-type Bac7(1−16) or the mono-substituted B7-001 and B7-002. The lower MIC value against *E. coli* BW25113 observed for the purified Bac7(1−16) (2 μM) with respect to that obtained by SPOT-synthesis (8 μM) may be due to lower purity level resulting from the SPOT-synthesis technique. We simultaneously determined whether the Bac7(1−16) derivatives exhibited differential susceptibility to degradation by blood serum proteases compared to the native Bac7(1−16) and thereby if they lose their antimicrobial properties. MIC assays carried out using the *E. coli* reference strain ATCC 25922 indicated that peptides B7-001, B7-002, and B7-003 as well as the wild-type Bac7(1−16) were fully active in the presence of serum (Table 2). On the other hand, three- and six-fold MIC increase was observed for B7-004 and B7-005, respectively. This result suggested that insertion of multiple W and/or R residues in the sequence might increase the susceptibility of the peptides to protease degradation. In parallel, the biocompatibility of Bac7(1−16) derivatives was evaluated using the human leukemia cell line MEC-1. Importantly, none of them displayed any significant toxicity, even at 64 μM after 24 h of exposure (Table 2 and Figure S1).

Broader Spectrum of Activity of the Selected Derivatives. Despite all the Bac7(1−16) derivatives having a similar efficacy against *E. coli*, their mode of action or their spectrum of activity could have changed compared to the wild-type peptide. Initially, we verified if Bac7 derivatives still

Table 3. MIC and MBC of Substituted Bac7 Peptides on Reference and Pathogenic Strains[a]

bacteria	B7 derivatives MIC (μM)						B7 derivatives MBC (μM)					
	wt	001	002	003	004	005	wt	001	002	003	004	005
E. coli BW25113[b]	3	1	1	2	2	2	4	1	8	4	8	4
E. coli BW25113Δ*sbmA*	16	12	4	16	3	4	64	32	16	32	4	4
E. coli ATCC 25922[b]	1	1	1	1.5	1	1	2	2	2	2	2	2
K. pneumoniae ATCC 700603	4	16	2	8	4	2	64	64	16	32	32	8
A. baumannii ATCC 19606	32	32	12	32	32	4	>64	64	24	64	32	8
P. aeruginosa ATCC 27853	>64	>64	>64	>64	64	32	>64	>64	32	>64	64	>64
S. aureus ATCC 25923	>64	>64	>64	>64	32	12	>64	>64	>64	>64	>64	>64

[a]Results are the median of at least three independent experiments (n = 3). The unmodified Bac7(1−16) (wt) was used for comparison. [b]MIC data on *E. coli* BW25113 and *E. coli* ATCC 25922 were reported here from Table 2 for comparison.

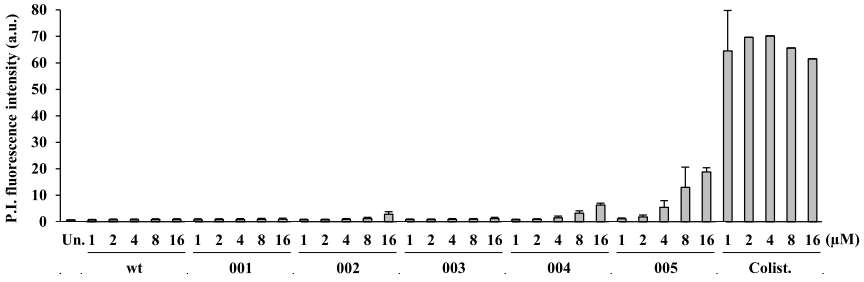

Figure 2. Assessment of *E. coli* BW25113 membrane permeabilization by flow cytometry. The uptake of PI was checked after incubating bacteria for 30 min in the presence of increasing peptide concentrations evaluating the median fluorescence intensity (MFI) of P.I.-positive bacteria. As a reference for permeabilization, the lytic peptide antibiotic colistin (Colist.) was used. Bacteria were treated with sterile water as untreated control (Un.). Reported data are the average and standard deviation of three independent experiments.

exploited the bacterial transporter SbmA to be fully active.[5] To do this, the MIC and minimum bactericidal concentration (MBC) of the Bac7(1−16) derivatives were determined against the SbmA null mutant *E. coli* strain BW25113Δ*sbmA*. Interestingly, B7-002, and especially B7-004 and B7-005, displayed very little difference (2−4-fold) in MIC and MBC between the wild-type and Δ*sbmA* strains (Table 3), whereas, by contrast, Bac7(1−16) showed a 16-fold increased MBC in the absence of SbmA. These data suggest that B7-004, B7-005, and partially B7-002 are almost fully independent of the SbmA transporter for their mode of action.

As some pathogens are naturally resistant to Bac7 fragments, most likely because of the absence of SbmA,[3] we hypothesized that the new derivatives could be active against bacterial species that do not express SbmA homologues. Therefore, the Bac7(1−16) derivatives were tested against reference strains of *P. aeruginosa* and *S. aureus* (which do not express proteins similar to SbmA) as well as *K. pneumoniae* and *A. baumannii* which possess an SbmA homologue.[3] We observed that the same derivatives that killed *E. coli* despite the absence of the membrane transporter also displayed a broadened spectrum of susceptible species. Interestingly, B7-002, B7-004, and B7-005 gained antimicrobial activity against *P. aeruginosa*; B7-004 and especially B7-005 also inhibited *S. aureus*, two species that are not susceptible to the unmodified Bac7(1−16). In addition, B7-004 and B7-005 displayed higher antimicrobial activity against *K. pneumoniae* and *A. baumannii* than Bac7(1−16) (Table 3). These results indicate that these new derivatives can affect a wider number of pathogenic species and do not need the presence of the transporter SbmA. We also tested the efficacy of Bac7(1−16) derivatives against clinical isolates of pathogenic *E. coli*. Each of the Bac7(1−16) derivatives displayed an MIC of 1 μM against all the strains, with the only exception of the *E. coli* EURL-VTEC C07 in which the MIC was >64 μM for the unmodified Bac7(1−16) but 2 μM for the tetra-substituted B7-005 (Table S2).

Membrane Permeabilizing Effect of Substituted Bac7(1−16) Peptides toward *E. coli* Cells. The low dependency on SbmA displayed by some Bac7(1−16) derivatives indicated that they can cross the membrane using a different mechanism. Indeed, the introduction of additional Arg and Trp residues in the sequence suggests that the peptides may have gained the ability to directly interact with the bacterial membranes. To assess this possibility, propidium iodide (PI) uptake and ONPG/β-galactosidase assays were performed. The PI-fluorescence associated with *E. coli* BW25113 cells treated with each of the Bac7(1−16) derivatives, evaluated by flow cytometry, was taken as an indicator of the extent of membrane permeabilization (Figure 2). Similarly, the chromogenic hydrolysis of the ONPG, occurring only if the cytosolic β-galactosidase was unmasked, was taken as indicator that the membrane of *E. coli* ML-35 was damaged (Fig. S2). The bacterial membrane of *E. coli* BW25113 cells appeared unchanged in the presence of the wild-type Bac7(1−16) as well as of the peptides B7-001, -002, and -003. A detectable increase in fluorescence was observed in the presence of 8 and 16 μM of B7-004 and B7-005. The latter peptide also facilitated PI-uptake appreciably at 4 μM. These results revealed that B7-004, and especially B7-005, had gained the capability to alter the membrane integrity (Figure 2). Comparable results were obtained also by the ONPG assay (Figure S2). The similar trend between the decreased dependency on SbmA and the membrane-perturbing activity of B7-004 and B7-005 suggested that these peptides acquired the capability to interact with the membrane and perhaps to cross it. However, the highest PI-fluorescence value detected after the treatment with the two peptides at 16 μM was only ≈30% or below of that measured in the presence of the

membranolytic peptide antibiotic colistin at 1 μM. In addition, no increase in fluorescence was induced by any of the peptides at their MICs (1−2 μM, Table 2). Overall, the weak membranolytic effect of both B7-004 and B7-005 when compared to that of colistin and of other membrane-destroying AMPs (e.g., melittin[31]) suggests that their killing activity is not based on the permeabilization of the bacterial membranes.

Inhibitory Activity of Substituted Bac7(1−16) Derivatives *in Vitro*. To directly assess if the Bac7(1−16) derivatives maintained the same mechanism of protein synthesis inhibition as the parent peptide,[3,11] we performed *in vitro* transcription/translation assays using *E. coli* lysates. As expected, the unmodified Bac7(1−16) was shown to be an excellent inhibitor of protein synthesis with 90% inhibition observed at 1 μM and complete inhibition at >5 μM concentrations (Figure 3). The mono-substituted peptide B7-001 exhibited a slight reduction in inhibitory activity at 1 μM compared to the wild-type, whereas the effect of the mono-substituted B7-002 was very similar to that of Bac7(1−16). The di-substituted B7-003 was a significantly weaker inhibitor of the *in vitro* transcription-translation, despite its MIC value being only twofold higher than that of Bac7(1−16) (see Table 2). Tri- and tetra-substituted B7-004 and B7-005 displayed slightly decreased inhibitory activity compared with that of the wild-type peptide (Figure 3).

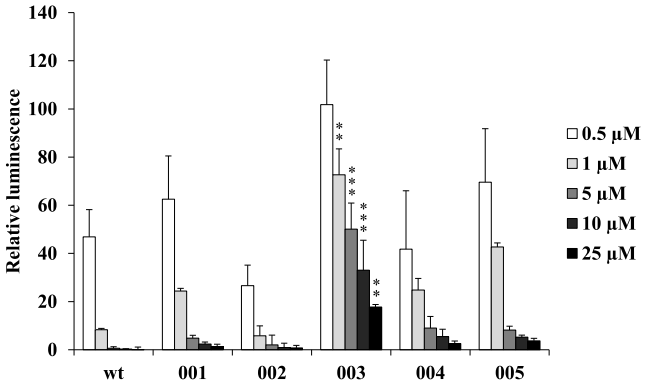

Figure 3. Luciferase activity after *in vitro* transcription/translation reactions. *E. coli* lysates were treated with increasing concentrations of modified PrAMPs. Results are presented as the percentage of control samples treated with only RNase free water. Average and standard deviation of at least five independent experiments (n = 5). Student's t-test for each concentration of B7-003 vs the same concentration of all the other derivatives, ** = p-value < 0.01, *** = p-value < 0.001.

Overall, only B7-003 clearly reduced its effect on the bacterial translation, without losing its antibacterial activity on living bacteria. B7-003 was not-permeabilizing (Figures 2 and S2) and still relied on SbmA to inhibit the bacterial growth (Table 3), suggesting an intracellular mode of action. We hypothesized then that B7-003 could display weak or peculiar interactions with the ribosome, thereby explaining its dissimilar inhibition of protein synthesis compared to the other derivatives.

Crystal Structures of Bac7(1−16) Derivatives in Complex with the 70S Ribosome. To understand how the substitutions within mono- and multi-substituted Bac7(1−16) derivatives influence ribosome binding, the structures of Bac7(1−16) derivatives in complex with the *Thermus thermophilus* 70S ribosome were analyzed and compared to that of Bac7(1−16).[11,13] We obtained satisfactory electron density maps (Figure S3A−D) and built corresponding structures of B7-001 and B7-002 in complex with the ribosome at 3.0 and 3.05 Å resolution, respectively (Figure 4A−C). The quality of the electron density map allowed the building of molecular models for both of the peptides with the side chains for residues 1−15, with the overall conformation and interactions within the ribosomal tunnel very similar to that reported previously for Bac7(1−16)[11,13] (Figure S4B,C). By contrast, despite numerous attempts, we were not able to obtain electron density maps with sufficient detail for the ribosome-bound multi-substituted B7-003, B7-004, and B7-005 peptides. From the few low-resolution datasets, we could infer that all the peptides have the same overall binding site in the nascent peptide exit tunnel within the *T. thermophilus* 70S ribosome (Figure S5A−C). However, the details of their interactions with the ribosome could not be deciphered. This may be due to the increased charge of the multi-substituted peptides that interfered with crystal packing and/or to the weak binding affinity of those peptides to *T. thermophilus* ribosomes.

The side-chain of Arg1 in the Bac7(1−16) formed two hydrogen bonds (H-bonds) with the nucleotides U2555 and C2556 of the 23S rRNA.[11] Substitution of R1W in B7-001 led to a loss of the H-bonds, suggesting that they are not critical for activity. This is consistent with the observation that Bac7(1−16) derivatives with substitutions of Arg1 to Ala, Gly, or Pro still retained excellent antimicrobial activity (see Table 1). Nevertheless, the loss of H-bonding in B7-001 appeared to be compensated by stacking interactions between the Trp1 and the base of U2555 and the ribose of U2556 (Figure 4D). In the unmodified peptide, Pro15 did not establish any interactions with components of the ribosomal tunnel,[11] whereas the substitution of P15W in B7-002 generates additional stacking interactions between the side-chain of Trp15 and the base-pair between nucleotides A752 and U2609 of the 23S rRNA (Figure 4E). This additional interaction may contribute to its slightly increased antibacterial activity against *E. coli* BW25113 (see Table 2) compared to the unmodified peptide.

MD of Noncrystallized Bac7(1−16) Derivatives in Complex with the 70S Ribosome. To predict at atomic level the details of the interactions between the ribosome and the Bac7 (1-16) derivatives that were not described in detail by X-ray crystallography, cumulative 600 ns-long MD simulations of the ribosomal 50S subunit model in explicit water solvent (a total of 1,350,000 atoms) were performed. The flexibility was measured for all the simulated peptides by monitoring the root-mean-square fluctuation (RMSF) per residue, assuming that low flexibility likely indicates stable binding of the peptide to the ribosome. Models of B7-003, -004, and -005 displayed an RMSF profile similar to that of the original Bac7(1−16) (Figure S6), so they were predicted to bind the ribosomal exit tunnel similarly to the unmodified peptide. As a control, the Bac7(1−16) derivatives B7-R9G and B7-P13E, showing very poor antimicrobial activity (Table 1), were also simulated and displayed an RMSF profile quite different from that of the unmodified Bac7(1−16) and the B7-003, -004, and -005 derivatives (Figure S6), pinpointing a remarkably higher flexibility and suggesting poorer binding. The low-resolution data provided by crystallographic studies were therefore supported and expanded by mapping the interactions of the peptide residues (Figure 5). In the peptide B7-003, the W13 (substitution P13W) did not interact with the surrounding rRNA nucleobase, most probably because of the

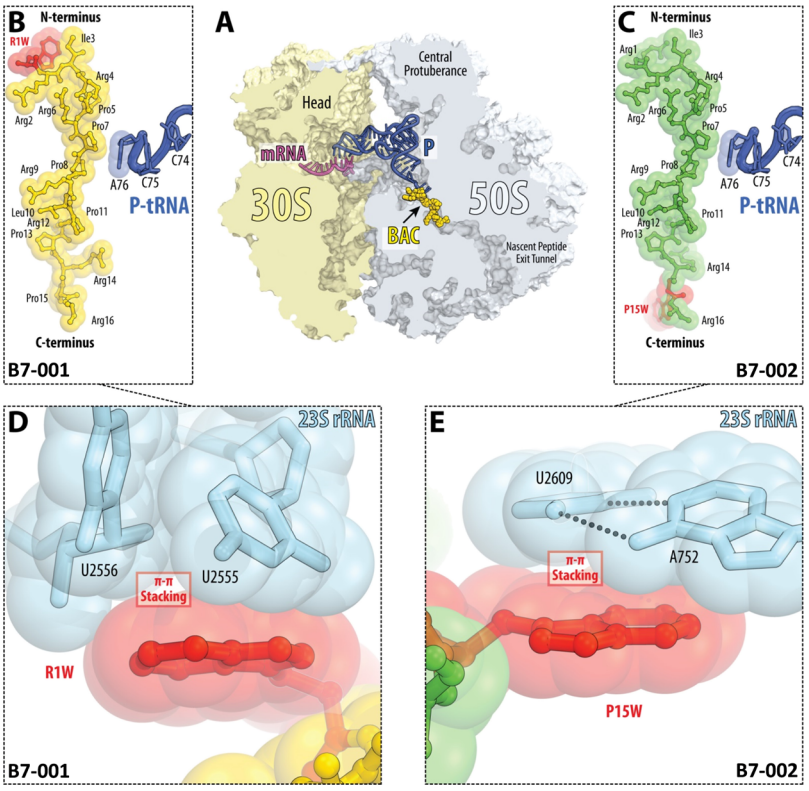

Figure 4. Structure of B7-001 and B7-002 in complex with the *Tth* 70S ribosome and P-site tRNA. (A) Overview of the Bac7 binding site (yellow) in the *T. thermophilus* 70S ribosome viewed as a transverse section through the nascent peptide exit tunnel. The 30S subunit is shown in light yellow, the 50S subunit is in light blue, and the mRNA and the P-site tRNA are magenta and dark blue, respectively. (B,C) Close-up views of the B7-001 (yellow, B) and B7-002 (green, C) binding sites relative to the P-site tRNA (dark blue). Note that in the presence of Bac7(1−16) derivatives, nucleotide A76 of the P-site tRNA flips out by about 180° into a new conformation, in which it no longer forms H-bond interactions with A2451 and the A-site substrate that are required for efficient peptide bond formation. (D,E) Detailed views of the interactions between the mutated residues R1W (red, D) in B7-001 (yellow) or P15W (red, E) in B7-002 (green) with the indicated nucleotides of the 23S rRNA. PDB entry for starting structure: 4Y4P.

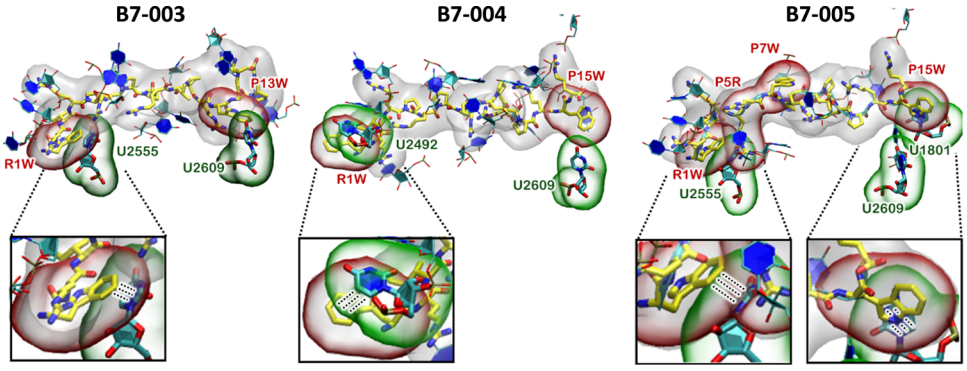

Figure 5. Binding poses of the peptides B7-003, B7-004, and B7-005 (space filling and sticks) as extracted from a cluster analysis of the MD simulation trajectories. For clarity, only the nucleotides of the *T. thermophilus* ribosomal exit tunnel interacting with the peptides are shown and represented as licorice with carbon atoms depicted in yellow (peptide) and cyan (ribosome), while oxygen and nitrogen atoms are displayed in red and blue, respectively. Mutated peptide residues are encircled in a red surface, and surrounding interacting RNA nucleotides are highlighted in a green surface. Dashed lines depict π-stacking interactions. PDB entry for starting structure: 5F8K.

structural rearrangement induced by the π-stacking interaction of W1 with the U2555 residue of the ribosomal tunnel (Figure 5). Similarly, the substitution R1W appeared to impair the interaction of W15 with U2609, as observed for the peptide B7-004 (Figure 5). The interaction between W15 and surrounding nucleotides was partially restored in the peptide B7-005 where the interaction between W1 and U2555 was slightly weakened. This may be due to the rearrangements induced in B7-005 by the substitutions P5R and P7W (Figure 5). This systematic structural analysis delineates how gluing the N-terminus of the peptide may help in anchoring the peptide into the ribosome's tunnel, in line with the structural data shown above. Conversely, the substitution of further residues may destabilize the π-stacking interactions established by W1 decreasing the binding affinity of the peptide and its biological effect.

DISCUSSION

Currently, PrAMPs cannot fully address the clinical need for new antimicrobials. Their spectrum of activity is not broad enough for many general applications. Moreover, PrAMPs mainly rely on the nonessential bacterial membrane protein SbmA to be transported into the cell and consequently kill the microorganism. Bacteria can therefore potentially develop resistance against these compounds relatively easily by mutating the transporter. Moreover, the scarce knowledge of the structure−activity relationships that explain ribosome binding and protein synthesis inhibition by these peptides has so far prevented the optimization and rational design of more potent PrAMP derivatives. The identification of the Bac7(1−16) residues critical for interacting with the ribosome and facilitating the block of the bacterial protein synthesis and growth is therefore mandatory for any optimization of these peptides.

Here, we have shown that the short sequence $-_{9}RLP_{11}-$ is crucial for the inhibitory activity of Bac7(1−16) against *E. coli* protein synthesis and viability (see Figure 1). The importance of these residues for the mechanism of action of Bac7(1−16) is also supported by our structural studies. The position of the lateral chains of these residues was almost perfectly superimposable in all the crystals obtained in this study, suggesting that they form crucial interactions with the ribosome (Figure S4). The only substitution in the $-_{9}RLP_{11}-$ region that did not impair the antimicrobial activity of Bac7(1−16) was that with Trp, which was well tolerated also along the whole sequence of Bac7(1−16). In a few cases, the exchange of some single residues of the native peptide with Trp even improved the activity of the peptide (Tables 1 and 2). A similar effect had been reported also for the derivatives of the mammalian PrAMPs Bac5(1−17).[22] The boosting effect of Trp on the activity of PrAMPs is therefore intriguing also because this amino acid is rarely represented in the known sequence of native PrAMPs.[4] We recently reported that the Tur1B, a PrAMPs isolated from the dolphin *Tursiops truncatus*, has four Trp residues in its 32 residue-long sequence. However, this peptide did not exhibit a strong inhibitory effect on protein synthesis.[16] Other cetacean PrAMPs recently identified from protein sequence databases show a high number of tryptophans (Sola R., unpublished results), suggesting that introduction of Trp has already occurred during evolution.

The antimicrobial effect and the inhibition of protein synthesis activity observed here studying mono- and multi-substituted Bac7(1−16) derivatives was used to generate a consensus sequence highlighting the Bac7(1−16) residues that are essential for the inhibition of the protein synthesis (Figure 6). Subsequently, to identify the residues needed by PrAMPs to inhibit the bacterial ribosome in a more general context, we extended the consensus to other PrAMPs that are known to block the protein synthesis and that were crystallized in the ribosomal exit tunnel, that is, the dolphin-derived Tur1A[16] and the insect-derived Onc112,[12] Pyrrhocoricin, and Metalnikowin-1[11] (Figure 6). The sequences of these peptides were therefore manually aligned using common features, which were then combined with the collected functional data to identify the key residues.

According to our alignment, the N-terminal residues of Bac7(1−16) and Tur1A, although per se important for the antimicrobial activity of the peptide and for its efficacy on the bacterial protein synthesis,[11,16] did not display any similarity

Peptide	Sequence
Bac7(1-16)	RRIRPRPPRLPRPRPR
B7-001	WRIRPRPPRLPRPRPR
B7-002	RRIRPRPPRLPRPRWR
B7-003	WRIRPRPPRLPRWRPR
B7-004	WRIRRRPPRLPRPRWR
B7-005	WRIRRRWPRLPRPRWR
Tur1A	RRIRFRPPYLPRPGRR...
Onc112	VDKPPYLPRPRPPRrIYNr-NH_2
Pyrrhocoricin	VDKGSYLPRPTPPRPIYNRN
Metalnikowin-1	VDKPDYRPRPRPPNM
PrAMPs consensus	**+XX*LPRPRX**

Figure 6. Sequence alignment of Bac7(1−16) derivatives with mammalian and insect PrAMPs binding the ribosomal exit tunnel.is rarely represented in the known B7-003, the only Bac7(1−16) derivatives with strongly decreased inhibitory activity toward protein synthesis, is highlighted in gray. * indicates R or Y.

with the sequences of the insect-derived PrAMPs. The first aligned residues of the consensus are the positively charged R_6 in mammalian PrAMPs and K_3 in insect PrAMPs. Most of the Bac7(1−16) residues R_9−R_{14}, shared by Bac7(1−16) derivatives effectively inhibiting bacterial growth and protein synthesis, were very conserved also among insect-derived PrAMPs (Figure 6). Interestingly, with regard to the R9 of Bac7(1−16) and its derivatives, all the other PrAMPs have a Tyr (Y) in that position, regardless of their mammalian or insect origin (Figure 6). This is reasonable as the space-filling of the lateral chains of Arg and Tyr is quite similar. Both the guanidino group of Arg and the phenolic group of Tyr are quite bulky and planar, allowing similar interactions by π-stacking with the surrounding environment in the ribosomal exit tunnel. It is worth noting that the PrAMPs consensus that we propose is in agreement with the results of previous studies on the insect-derived PrAMPs pyrrhocoricin[32] and oncocin[33] as the residues highlighted in the consensus (+XXR/YLPRPRX) have been shown experimentally to be essential for the antimicrobial effect of these peptides. We believe that the PrAMPs consensus may be instrumental to design new PrAMP derivatives maintaining a good efficacy in inhibiting the bacterial protein synthesis.

Looking then at the antibacterial potential of Bac7(1−16) derivatives, apparently none of the five peptides was endowed with higher antimicrobial activity against the reference *E. coli* strains used for the screening (Table 2). Nevertheless, the derivatives with an increased number of Arg and Trp, B7-004 and especially B7-005, displayed substantial improvements compared to the parent molecule. They exhibited (i) wider spectrum of activity including Gram-positive strains and higher activity against Gram-negative as well as (ii) limited dependency on the bacterial transporter SbmA, suggesting a distinct mode to enter the bacterial cells.

Both B7-004 and B7-005 remained effective inhibitors of the bacterial protein synthesis, but at the same time they acquired the tendency to interact, and to moderately perturb, the bacterial membrane as they slightly increased its permeability. The high number of Arg and Trp residues could explain this feature, possibly strengthening the interaction of B7-004 and B7-005 with the membranes and promoting their passage

through the phospholipid bilayer. The reduced dependency of B7-004 and B7-005 on SbmA is an important advantage for these molecules because in principle it makes it more difficult for bacteria to resist their antimicrobial effects. The mutational inactivation of SbmA would indeed not affect the bacterial sensitivity to B7-004 and B7-005, differently to what has been observed for other native PrAMPs.[5,34] A strong interaction with the membrane is usually accompanied by a reduced selectivity for the target and an increase of cytotoxicity.[35] By contrast, here we observed that the multi-substituted peptides displayed the same high biocompatibility of the native Bac7(1−16).

The increased capability of Bac7(1−16) derivatives to alter the membrane permeability may explain the broadened spectrum of activity displayed by B7-004 and B7-005 and partially by B7-002. The peptides not only increased their bactericidal effects against pathogens sensitive to native PrAMPs, such as pathogenic *E. coli* strains, *K. pneumoniae,* and *A. baumannii* strains, but also gained antimicrobial activity against bacterial species, for example, *P. aeruginosa* and *S. aureus* (Table 3), which are not susceptible to the unmodified Bac7(1−16).[4] Indeed, both *P. aeruginosa* and *S. aureus* do not express SbmA and are much less sensitive to native PrAMPs than the *Enterobacteriaceae*[19,20] as the peptides cannot easily penetrate inside their cytosol. Against these pathogens, PrAMPs can exert only a moderate antibacterial effect, mainly by membrane destabilization, as observed, for example, for *P. aeruginosa*.[36]

CONCLUSIONS

In summary, B7-005 combines good antibacterial features with the lack of toxic effects against eukaryotic blood cells at concentrations much above its MIC and MBC against many pathogenic strains and with a valuable antimicrobial effect in the presence of human serum. The tolerance of B7-005 against serum proteases is a further optimistic indication that this peptide could be effective to fight a critical clinical condition, such as bacteraemia, which needs rapid and broad-range antibiotic treatment. This derivative could resist these proteolytic enzymes that represent a big threat for PrAMPs and for AMPs in general.[37−39] B7-005 overcomes therefore some of the major limits of the native PrAMPs. This peptide gets closer to becoming a lead compound for a broad-range antimicrobial to be used as a first line of defence against most of the ESKAPE pathogens, considered by the World Health Organization to be a serious threat for human health. Moreover, we propose a consensus that could drive the design of new PrAMP derivatives preserving their capability to inhibit the protein synthesis.

EXPERIMENTAL SECTION

Peptide Synthesis. Peptide libraries were synthesized by automated solid-phase peptide synthesis on a Whatman 50 cellulose membrane using an automated MultiPep RSI peptide (Intavis), adapting the manual synthesis protocol described in ref 40. Briefly, the cellulose membrane (10 cm × 15 cm) was functionalized by overnight incubation in 0.2 M Fmoc-Gly-OH (Aldrich), 0.24 M *N,N′*-diisopropylcarbodiimide (DIC, Fluka), and 0.4 M *N*-methylimidazole (Aldrich) in dimethylformamide (DMF, VWR) before automated synthesis. Subsequently, the glycine was deprotected in 20% piperidine (v/v, Acros Organics) in DMF (20 + 10 min). Peptide synthesis at discrete spots was performed using 9-fluorenylmethoxycarbonyl/*tert*-butyl (Fmoc/*t*Bu) strategy. Fmoc amino acids [Bachem, 0.5 M stock solutions in *N*-methyl-2-pyrrolidone (NMP, VWR)] were preactivated with equimolar quantities of 1-hydroxybenzotriazole hydrate (HOBt, Aldrich) and DIC (both 1.1 M stock solutions in NMP) and performed by double coupling procedure (2 × 10 min) to guarantee a higher coupling efficiency at each position of the amino acid sequence. The spotting volumes were 0.8 μL for the first cycle and 0.9 μL for the following cycles. After each amino acid coupling cycle, a 5 min acetic anhydride treatment (5% v/v in DMF, Fluka) was employed to cap unreacted residues. Subsequently, the Fmoc protection group was cleaved using 20% (v/v) piperidine in DMF (2 × 5 min). Final cleavage of amino acid side-chain protecting groups was carried out with 25 ml of 90% trifluoroacetic acid (TFA) (Acros Organics), 3% tri-isopropylsilane (TIPS, Acros Organics), and 2% water in dichloromethane (DCM, Acros Organics) for 30 min, followed by a 120 min treatment with 25 ml of 50% TFA, 3% TIPS, and 2% water in DCM. An overnight incubation in a saturated ammonia gas atmosphere cleaved the peptide amides from the solid support. To determine SPOT synthesis yield and quality, an internally standardized control peptide and individually chosen peptides from that synthesis were used. Using a one-hole puncher (Ø = 6 mm), individual SPOTs were punched out, transferred into a sterile 96-well round-bottomed polypropylene nontreated microtiter plate, and dissolved overnight in 200 μL of sterile water at room temperature. Peptides' concentration was quantified measuring the absorbance at 280 nm using a NanoDrop ND1000 spectrophotometer. The same peptides were then analyzed by analytical RP-HPLC on a Shim-pack VP-ODS column (120 Å, 150 × 4.6 mm, Shimadzu) using a LC2010AHT system (Shimadzu). The solvents used were 0.01% (v/v) TFA in H_2O (HPLC-grade, VWR, solvent A) and 0.01% (v/v) TFA in acetonitrile (HPLC-grade, VWR, solvent B). A linear gradient of 5−70% of solvent B in 32.5 min with an initial 3 min isocratic equilibration and a flow rate of 1 mL/min were used. The purity of the crude control peptides was between 37 and 68%. The remaining spots were then excised from the membrane at room temperature, placed in microtiter plates, and the cleaved peptides resuspended overnight in 200 μL of sterile water, lyophilized, and re-lyophilized from 200 μL of 10 mM HCl solution to remove TFA. The peptide pellets were resuspended in 50 μL of sterile water and quantified spectrophotometrically using a Nanodrop2000 measuring the absorbance at 214 nm by a spectrophotometer. The molar coefficient at 214 nm of each peptide was calculated using the in house program ConCalc using the values reported in ref 41.

Larger amounts of the best candidate peptides (B7-001 -002 -003 -004 -005) were synthesized by solid-phase synthesis using Fmoc chemistry, purified by reverse-phase HPLC to the final purity ≥95% and controlled by mass spectrometry. These peptides were purchased from NovoPro (China), lyophilized three times from 10 mM HCl to remove TFA, and quantified as reported above.

Bacterial Culture. The bacterial strains used in this work were *E. coli* BW25113, *E. coli* BW25113Δ*sbmA* (JW0368-1, KEIO collection[42]), *E. coli* ML-35, *E. coli* ATCC 25922 *K. pneumoniae* ATCC 700603, *A. baumannii* ATCC 19060, *S. aureus* ATCC 25923, and *P. aeruginosa* ATCC 27853. The *E. coli* pathogenic strains (*E. coli* EC1 ÷ 6) were generously provided by the European Union Reference Laboratory for *E. coli* Department of Food Safety, Nutrition and Veterinary Public Health, Istituto Superiore di Sanità, Rome, Italy. All the bacterial strains used in this study were grown overnight at 37 °C in Müller−Hinton broth (MHB, Difco) with shaking (140 rpm); then, the day after, the bacterial cultures were diluted approx. 1:40 in fresh MHB and incubated at 37 °C with shaking (140 rpm) to mid-log phase, until an optical density (OD) at 600 nm (OD_{600}) ≈ 0.3 was reached. Kanamycin (50 μg/mL) was added to the medium for *E. coli* BW25113Δ*sbmA*.

Minimum Inhibitory Concentration Determination. Mid-log bacterial cultures were diluted to 5 × 10^5 colony-forming units (cfu)/mL in MHB. The peptides, diluted in MHB to the concentration of 128 μM, were added to the first wells of a round-bottom 96-well microtiter plate and serially twofold diluted in a final volume of 50 μL of MHB into successive wells. Subsequently, 50 μL of the bacterial suspension 5 × 10^5 cfu/mL (see above) was added to each well. This reduced the final bacterial load to 2.5 × 10^4 cfu/well and halved the

peptide concentration in the wells. The same amount of untreated bacteria in MHB was used as bacterial growth control. MHB (100 μL) was used to control the medium sterility. The plate was sealed with Parafilm to minimize evaporation and incubated overnight at 37 °C (for approx. 18 h). The MIC was calculated as the lowest compound concentration preventing visible bacterial growth in the wells. In the case of barely detectable growth in the wells, the OD_{620nm} of the plate was measured using a multiplate reader Tecan equipped with Sunrise software. The MIC was then calculated as the well whose OD_{620} was reduced by 99% or more, compared to that of the untreated control.

For the MIC assays in the presence of human serum, six anonymous blood samples of healthy donors (generous gift of the Blood Bank of the University Hospital "Ospedale Maggiore" of Trieste, Italy) were pooled. After clotting at room temperature, the clot was removed by centrifugation (2000*g*, 10 min). The serum was filtered using in sequence 0.4 μm and 0.22 μm filters, aliquoted aseptically, and stored at −20 °C.

Data are reported as median of independent experiments repeated three times or four times in case of uncertain values.

Cell Toxicity Assay. Cytotoxicity assays were performed by the tetrazolium salts test (MTT), exposing the human cell line of lymphocytes B precursors MEC-1 to peptides and sterile water as a control at 37 °C and 5% CO_2. MEC-1 cells were grown in RPMI (Sigma) + 10% fetal bovine serum (Sigma) + 2 mM glutamine (Sigma) + 100 U/mL penicillin (Sigma) + 100 μg/mL streptomycin (Sigma). Cells were then counted and diluted to 2×10^6 cell/mL. Twofold serial dilutions of the peptides were prepared in 50 μL of cell growth medium in a 96-flat-bottom microtiter plate (Euroclone); then 10^5 cells were added to each well in a volume of 50 μL in each well, reaching a final volume of 100 μL. As untreated controls, samples received only sterile water. Following 20 h of exposure to the compounds, 25 μL of an MTT solution (in sterile PBS) was added to each well to reach a final concentration of 1 mg/ml. After 4 h of incubation at 37 °C in the dark, 100 μL of Igepal (Sigma-Aldrich) 10% in 10 mM HCl (w/v) was added to each well, and the plate was incubated overnight at 37 °C. After approx. 18 h, the OD_{570nm} of the wells was measured on a plate-reader spectrophotometer Nanoquant infinite M200pro (Tecan). The peptide cytotoxicity was calculated comparing the OD_{570nm} of the treated samples with that of the untreated control. Data are reported as the average ± standard deviation of three independent experiments in single (n = 3) or duplicate (n = 6).

Assessment of Bacterial Membrane Integrity. For PI uptake assay, mid-log *E. coli* BW25113 cultures prepared as above were diluted to 5×10^5 cfu/mL in MHB added with a final concentration of 10 μg/mL PI (Sigma), then incubated at 37°, 200 rpm for 30 min in the presence of 1, 2, 4, 8, and 16 μM peptides or colistin sulfate (Sigma) as a control for membrane permeabilization. As untreated controls, bacterial samples were treated with sterile water only. The uptake of PI was evaluated by flow cytometry performed on an MACSQuant Analyzer 10 (Milteny Biotec) equipped with a laser 488 nm to assess the PI fluorescence. Results are expressed as MFI of PI of three independent experiments, collecting for each sample 20,000 events. Data were analyzed with FlowLogic software (version 7.2.1, Inivai Technologies). The results are the average of three independent experiments.

For ONPG/β-galactosidase assay, mid-log *E. coli* ML-35 cultures prepared as above were centrifuged (2000*g*, 10 min), resuspended in PBS to 10^7 cfu/mL, added with a final concentration of 1.5 mM *ortho*-nitrophenyl-β-galactoside (ONPG) (Sigma), and incubated at 37 °C for 30 min in the presence of 1, 2, 4, 8 , and 16 μM peptides or colistin sulfate (Sigma) as a control for membrane permeabilization. As untreated controls, bacterial samples were treated with sterile water. The chromogenic hydrolysis of the ONPG, occurring if the cytosolic β-galactosidase was unmasked by breaches in the bacterial envelope, was evaluated measuring the OD at 405 nm in a 96-well flat-bottom microtiter plate using an Infinite200Pro plate reader (Tecan). The blank (absorbance of untreated bacteria) was subtracted from the treated samples. Three independent experiments were performed as internal duplicate (n = 6).

***In Vitro* Transcription/Translation Assay.** *E. coli* lysate-based coupled transcription-translation assays (RTS100, BiotechRabbit) were performed as described previously for other PrAMPs.[11,12,15,16,22,43] Briefly, 6 μL reactions, with or without Bac7(1−16) peptide, were mixed according to the manufacturer's instructions and incubated for 1 h at 30 °C with shaking (750 rpm). The reaction was then stopped by adding 5 μL of kanamycin (50 μg/μL). All samples were diluted with 40 μL of Luciferase assay substrate (Promega) into a white 96-well chimney flat bottom microtiter plate (Greiner). The luminescence was then measured using a Tecan Infinite M200 plate reader. The relative values were determined by defining the luminescence value of the sample without inhibitor as 100%. All the experiments were performed in independent tri-replicates.

Crystallographic Structure Determination. All chemicals were from Sigma-Aldrich, except for PEG-20k and MPD, which were purchased from Hampton Research. All solutions were made with ultrapure water and filtered through 0.22 μm membranes before use. *E. coli* $tRNA_i^{Met}$ was kindly provided by Dr. Andrey L. Konevega and stored in water at −80 °C. Short mRNAs were ordered from IDT-DNA (Coralville, IA, USA) and stored in the *Tth* ribosome buffer (5 mM HEPES-KOH pH 7.5, 50 mM KCl, 10 mM NH_4Cl, 10 mM $Mg(CH_3COO)_2$, 0.6 mM β-mercaptoethanol) at −80 °C.

Ribosome complexes containing mRNA and P-site $tRNA_i^{Met}$ were formed as described previously.[44] Bac7(1−16) variants were added to the preformed ribosome complexes to a final concentration of 100 μM prior to crystallization. All *Tth* 70S ribosome complexes were formed in the buffer containing 5 mM HEPES−KOH (pH 7.6), 50 mM KCl, 10 mM NH_4Cl, and 10 mM $Mg(CH_3COO)_2$, and then crystallized in the buffer containing 100 mM Tris−HCl (pH 7.6), 2.9% (w/v) PEG-20k, 7−12% (v/v) MPD, 100−200 mM arginine, 0.5 mM β-mercaptoethanol. Crystals were grown by the vapor diffusion method in sitting drops at 19 °C and stabilized as described previously[44] with Bac7(1−16) derivatives being added to the stabilization buffers (100 μM each). Diffraction data were collected using beamline 24ID-C and 24ID-E at the Advanced Photon Source (Argonne National Laboratory, Argonne, IL). A complete dataset for each ribosome complex was collected using 0.979 Å wavelength at 100 K from multiple regions of the same crystal using 0.3° oscillations. The raw data were integrated and scaled using the XDS software package.[45] All crystals belonged to the primitive orthorhombic space group $P2_12_12_1$ with approximate unit cell dimensions of 210 Å × 450 Å × 620 Å and contained two copies of the 70S ribosome per asymmetric unit. Each structure was solved by molecular replacement using PHASER from the CCP4 program suite.[46] The search model was generated from the previously published structures of *T. thermophilus* 70S ribosome with bound mRNA and tRNAs (PDB entry 4Y4P from ref 44). The initial molecular replacement solutions were refined by rigid-body refinement with the ribosome split into multiple domains, followed by positional and individual B-factor refinement using PHENIX.[47] Noncrystallographic symmetry restraints were applied to four domains of the 30S ribosomal subunit (head, body, spur, helix 44) and four domains of the 50S subunit (body, L1-stalk, L10-stalk, C-terminus of the L9 protein).

Atomic models for Bac7(1−16) derivatives were generated in COOT using standard *de novo* building of a peptide/protein molecule. The final models of the *T. thermophilus* 70S ribosome in complex with mRNA, initiator $tRNA_i^{Met}$ in the P site, and one of the Bac7(1−16) variants were generated by multiple rounds of model building in COOT,[48] followed by refinement in PHENIX.[47] All figures showing atomic models were generated using the PyMol software (www.pymol.org).

To measure the peptide concentration, the absorbance of 1 mM peptide solutions in *T. thermophilus* RB (as estimated from dissolved mass) was measured at 205 and 280 nm against *T. thermophilus* RB as blank. Peptide concentrations at 280 nm were calculated using the ProtParam tool on the ExPASy web server57. Peptide concentrations

at 205 nm were calculated using the Protein Parameter Calculator developed by Anthis and Clore58.

MD Simulations. We built models starting from the Gram-negative eubacteria *T. thermophilus* 70S ribosome crystal structure bound with Bac7(1−16) AMP solved at the average resolution of 2.8 Å (PDB entry 5F8K).[11] This structure comprises several RNAs and numerous proteins and ions. To study the behavior of Bac7 within the ribosome exit tunnel, we included in our model the ribosomal 50S subunit comprising 5S and 23S rRNAs, A- and P-tRNAs as well as 10 ribosomal proteins that are in direct contact with rRNA and tRNA, 1101 Mg^{2+}, 5 Zn^{2+}, and 1 K^+ ions (Figure S6). Other components of the 70S ribosome system are located far away from the ribosome exit tunnel and were not expected to affect Bac7 binding and were thus not included in the models. In addition to wt Bac7(1−16), three models of mutant Bac7 derivatives were considered: B7-003 (R1W, P13W), B7-004 (R1W, P5R, P15W), B7-005 (R1W, P5R, P7W, P15W). Two further peptides endowed with poor antimicrobial effect were also considered as controls, Bac7(1−16)R9G and Bac7(1−16)P13E, to have a comparison with molecules not expected to bind the ribosome. All mutations were inserted by using the tleap module of AmberTools 16.[49] MD simulations were performed with Gromacs 2016 software package.[50] The AMBER-ff12SB force field (FF) was employed for proteins,[51] while the ff99 + bsc0+χOL3 FF was used for RNAs[52] and additional modrna08 parameters for modified RNA nucleosides[53] as these are the most validated and recommended FFs for protein/RNA systems.[54] Mg^{2+} ions were described with the nonbonded fixed point charge FF due to Åqvist.[55] Na^+ and K^+ ions parameters were taken from Joung and Cheatham,[56] while Zn^{2+} ions were modeled with the cationic dummy atoms approach developed by Pang.[57] The system was embedded in a 10 Å layer of TIP3P[58] water molecules leading to a box of 260 × 220 × 276 Å, containing 1101 Mg^{2+} ions, 4 Zn^{2+}, 1 K^+, and 475 Na^+ counter ions counting up to 1,350,000 atoms. The topologies were built with AmberTools 16[49] and were subsequently converted in a GROMACS 2016 format using the software acpype.[59]

In all simulations, we have used a slow equilibration protocol recommended for protein/RNA MD simulations[54] and used for RNA/protein systems.[60] Namely, the systems went initially through a soft minimization using a steepest descent algorithm with a force convergence criterion set to 1000 kJ mol^{-1} nm^{-1}. Then, the models were smoothly annealed from 0 to 300 K with a temperature gradient of 50 K every 2 ns and for a total of 12 ns. In this phase, only water molecules and Na^+ ions were allowed to move, while the rest were subjected to harmonic position restraints with a force constant of 1000 kJ/mol nm^2. Once the temperature was raised up to 300 K, 20 ns of *NPT* simulations were conducted to stabilize the pressure to 1 bar by coupling the systems to a Berendsen barostat,[61] imposing the same restraints used in the heating phase. Temperature control at 300 K was achieved by stochastic velocity rescaling thermostat.[62]

Subsequently, the barostat was switched to Parrinello−Rahman,[63,64] and the position restraints on proteins and RNAs were restricted only to the backbone atoms. These were gradually decreased in three consecutive steps of 30, 10, and 10 ns each, during which the force constant was set to 1000, 250, and 50 kJ/mol nm^2, respectively. Finally, after an attentive equilibration protocol of ∼80 ns, all the restraints were released and the production runs were performed for ∼80 ns (for a total of ∼160 ns) for each of the subjected models. Productive MD simulations were performed on the canonical ensemble (*NVT*) using periodic boundary conditions. The LINCS algorithm[65] was used to constrain the bonds involving hydrogen atoms and the particle mesh Ewald method[66] to account for long-range electrostatic interactions with a cutoff of 10 Å. An integration time step of 2 fs was used in all simulations. The trajectories were inspected with the VMD software.[67] All analyses, including RMSFs, were done with cpptraj module of AmberTools 16[49] on the stripped trajectories without water and counter-ions. All analyses were performed on last 60 ns of production phase.

■ ASSOCIATED CONTENT

Supporting Information

The Supporting Information is available free of charge at https://pubs.acs.org/doi/10.1021/acs.jmedchem.0c00665.

Analysis of the effect of residue substitutions on the Bac7(1−16) antimicrobial activity, cytotoxicity of resin-synthesized peptides on MEC-1 cells, MIC on clinically isolated pathogenic *E. coli* strains, MIC and the MBC of Bac7(1−16) and derivatives on *E. coli* ML-35, membrane permeabilization evaluated by the ONPG/*β*-galactosidase assay on *E. coli* ML-35, electron density maps depiction and comparison of ribosome-bound Bac7(1−16) and derivatives, MD to simulate the binding affinity of peptides to the ribosome, and model of 50S ribosomal subunit used for MD simulation (PDF)

Crystal structures (ZIP)

Molecular dynamics data (ZIP)

■ AUTHOR INFORMATION

Corresponding Author

Marco Scocchi − *Department of Life Sciences, University of Trieste, 34127 Trieste, Italy*; orcid.org/0000-0003-1247-3641; Phone: +39 0405588704; Email: mscocchi@units.it

Authors

Mario Mardirossian − *Department of Medical Sciences, University of Trieste, 34125 Trieste, Italy*

Riccardo Sola − *Department of Life Sciences, University of Trieste, 34127 Trieste, Italy*

Bertrand Beckert − *Institut für Biochemie und Molekularbiologie, University of Hamburg, 20146 Hamburg, Germany*

Erica Valencic − *Institute for Maternal and Child Health-IRCCS "Burlo Garofolo", 30137 Trieste, Italy*

Dominic W. P. Collis − *TiKa Diagnostics Ltd., SW 17 0RE London, U.K.*

Jure Borišek − *CNR-IOM at SISSA, 34136 Trieste, Italy*

Federica Armas − *Department of Life Sciences, University of Trieste, 34127 Trieste, Italy*

Adriana Di Stasi − *Department of Life Sciences, University of Trieste, 34127 Trieste, Italy*

Jan Buchmann − *Institut für Biochemie und Molekularbiologie, University of Hamburg, 20146 Hamburg, Germany; Department of Biological Sciences, University of Illinois at Chicago, Chicago, Illinois 60607, United States*

Egor A. Syroegin − *Department of Biological Sciences, University of Illinois at Chicago, Chicago, Illinois 60607, United States*

Yury S. Polikanov − *Department of Biological Sciences and Department of Pharmaceutical Sciences, University of Illinois at Chicago, Chicago, Illinois 60607, United States*

Alessandra Magistrato − *CNR-IOM at SISSA, 34136 Trieste, Italy*

Kai Hilpert − *Institute of Infection and Immunology, St. George's, University of London, SW 17 0RE London, U.K.*; orcid.org/0000-0001-7131-0370

Daniel N. Wilson − *Institut für Biochemie und Molekularbiologie, University of Hamburg, 20146 Hamburg, Germany*; orcid.org/0000-0003-3816-3828

Complete contact information is available at: https://pubs.acs.org/10.1021/acs.jmedchem.0c00665

Author Contributions

M.M., M.S., D.N.W., K.H., A.M. conceived the study; M.M., R.S., B.B., E.V., D.W.P.C., J.B., F.A., A.D.S., J.B., E.A.S., Y.S.P., A.M. designed and performed the experiments; M.M., M.S., D.N.W., K.H., A.M., Y.S.P. wrote and edited the manuscript; MS supervised the whole project.

Notes

The authors declare no competing financial interest.

Coordinates and structure factors were deposited in the RCSB Protein Data Bank with accession codes: 7JQL for the *T. thermophilus* 70S ribosome in complex with Bac7-001, mRNA, and P-site tRNA; 7JQM for the *T. thermophilus* 70S ribosome in complex with Bac7-002, mRNA, and P-site tRNA. The authors will release the atomic coordinates and experimental data upon article publication.

■ ACKNOWLEDGMENTS

We thank all members of the D.N.W., M.S., and Y.S.P. laboratories for valuable suggestions. We thank A. Mankin for important discussions and critical feedback. We thank the staff at NE-CAT beamlines 24ID-C and 24ID-E for help with data collection and freezing of the crystals, especially Drs. K. Rajashankar, M. Capel, F. Murphy, I. Kourinov, A. Lynch, S. Banerjee, D. Neau, J. Schuermann, N. Sukumar, J. Withrow, K. Perry, and C. Salbego. This work is based upon research conducted at the Northeastern Collaborative Access Team beamlines, which are funded by the National Institute of General Medical Sciences from the National Institutes of Health [P30-GM124165 to NE-CAT]. The Pilatus 6M detector on 24ID-C beamline is funded by a NIH-ORIP HEI [S10 RR029205 to NE-CAT]. The Eiger 16M detector on 24ID-E beamline is funded by a NIH-ORIP HEI grant [S10 OD021527 to NE-CAT]. This research used resources of the Advanced Photon Source, a U.S. Department of Energy (DOE) Office of Science User Facility operated for the DOE Office of Science by Argonne National Laboratory under contract no. DE-AC02-06CH11357. This work was supported by Illinois State start-up funds to Y.S.P.. This project was supported by the Deutsche Zentrum für Luft-und Raumfahrt (DLR01Kl1820 to D.N.W.) within the "RIBOTARGET" consortium under the frame of JPIAMR. M.S. thanks Area Science Park for supporting with the "Made in Trieste project: research programmes among regional public bodies and companies". K.H. thanks the Institute of Infection and Immunity for a start-up grant.

■ ABBREVIATIONS

AMPs, antimicrobial peptides; cfu, colony-forming unit; Colist, colistin; DIC, *N*,*N*′-diisopropylcarbodiimide; FBS, fetal bovine serum; FF, force field; Fmoc/*t*Bu, 9-fluorenyl-methoxycarbonyl/*tert*-butyl; H-bonds, hydrogen bonds; HOBt, hydroxybenzotriazole; IDT-DNA, integrated DNA technologies; MBC, minimum bactericidal concentration; MFI, median fluorescence intensity; MHB, Müller−Hinton broth; MIC, minimum inhibitory concentration; MTT, 3-(4,5-dimethylthiazol-2-yl)-2,5-diphenyltetrazolium bromide; NMI, *N*-methylimidazole; PI, propidium iodide; PrAMPs, proline-rich antimicrobial peptides; RLU, relative light units; RMSF, root-mean-square fluctuation; RP-HPLC, reversed phase high-performance liquid chromatography; scr, scrambled; ser, serum; SPPS, solid-phase peptide synthesis; Un, untreated control; wt, unmodified peptide; PEG-20k, poly(ethylene glycol)M_n20,000; MPD, 2-methyl-2,4-pentanediol; *NVT*, number volume temperature.

■ REFERENCES

(1) Ventola, C. L. The antibiotic resistance crisis: part 1: causes and threats. *P T* **2015**, *40*, 277−283.

(2) Mishra, B.; Reiling, S.; Zarena, D.; Wang, G. Host defense antimicrobial peptides as antibiotics: design and application strategies. *Curr. Opin. Chem. Biol.* **2017**, *38*, 87−96.

(3) Graf, M.; Mardirossian, M.; Nguyen, F.; Seefeldt, A. C.; Guichard, G.; Scocchi, M.; Innis, C. A.; Wilson, D. N. Proline-rich antimicrobial peptides targeting protein synthesis. *Nat. Prod. Rep.* **2017**, *34*, 702−711.

(4) Scocchi, M.; Tossi, A.; Gennaro, R. Proline-rich antimicrobial peptides: converging to a non-lytic mechanism of action. *Cell. Mol. Life Sci.* **2011**, *68*, 2317−2330.

(5) Mattiuzzo, M.; Bandiera, A.; Gennaro, R.; Benincasa, M.; Pacor, S.; Antcheva, N.; Scocchi, M. Role of the Escherichia coli SbmA in the antimicrobial activity of proline-rich peptides. *Mol. Microbiol.* **2007**, *66*, 151−163.

(6) Paulsen, V. S.; Mardirossian, M.; Blencke, H.-M.; Benincasa, M.; Runti, G.; Nepa, M.; Haug, T.; Stensvåg, K.; Scocchi, M. Inner membrane proteins YgdD and SbmA are required for the complete susceptibility of Escherichia coli to the proline-rich antimicrobial peptide arasin 1(1-25). *Microbiology* **2016**, *162*, 601−609.

(7) Krizsan, A.; Knappe, D.; Hoffmann, R. Influence of the yjiL-mdtM gene cluster on the antibacterial activity of proline-rich antimicrobial peptides overcoming Escherichia coli resistance induced by the missing SbmA transporter system. *Antimicrob. Agents Chemother.* **2015**, *59*, 5992−5998.

(8) Krizsan, A.; Volke, D.; Weinert, S.; Sträter, N.; Knappe, D.; Hoffmann, R. Insect-derived proline-rich antimicrobial peptides kill bacteria by inhibiting bacterial protein translation at the 70S ribosome. *Angew. Chem., Int. Ed.* **2014**, *53*, 12236−12239.

(9) Mardirossian, M.; Grzela, R.; Giglione, C.; Meinnel, T.; Gennaro, R.; Mergaert, P.; Scocchi, M. The host antimicrobial peptide Bac71-35 binds to bacterial ribosomal proteins and inhibits protein synthesis. *Chem. Biol.* **2014**, *21*, 1639−1647.

(10) Taniguchi, M.; Ochiai, A.; Kondo, H.; Fukuda, S.; Ishiyama, Y.; Saitoh, E.; Kato, T.; Tanaka, T. Pyrrhocoricin, a proline-rich antimicrobial peptide derived from insect, inhibits the translation process in the cell-free Escherichia coli protein synthesis system. *J. Biosci. Bioeng.* **2016**, *121*, 591−598.

(11) Seefeldt, A. C.; Graf, M.; Pérébaskine, N.; Nguyen, F.; Arenz, S.; Mardirossian, M.; Scocchi, M.; Wilson, D. N.; Innis, C. A. Structure of the mammalian antimicrobial peptide Bac7(1-16) bound within the exit tunnel of a bacterial ribosome. *Nucleic Acids Res.* **2016**, *44*, 2429−2438.

(12) Seefeldt, A. C.; Nguyen, F.; Antunes, S.; Pérébaskine, N.; Graf, M.; Arenz, S.; Inampudi, K. K.; Douat, C.; Guichard, G.; Wilson, D. N.; Innis, C. A. The proline-rich antimicrobial peptide Onc112 inhibits translation by blocking and destabilizing the initiation complex. *Nat. Struct. Mol. Biol.* **2015**, *22*, 470−475.

(13) Gagnon, M. G.; Roy, R. N.; Lomakin, I. B.; Florin, T.; Mankin, A. S.; Steitz, T. A. Structures of proline-rich peptides bound to the ribosome reveal a common mechanism of protein synthesis inhibition. *Nucleic Acids Res.* **2016**, *44*, 2439−2450.

(14) Roy, R. N.; Lomakin, I. B.; Gagnon, M. G.; Steitz, T. A. The mechanism of inhibition of protein synthesis by the proline-rich peptide oncocin. *Nat. Struct. Mol. Biol.* **2015**, *22*, 466−469.

(15) Mardirossian, M.; Barrière, Q.; Timchenko, T.; Müller, C.; Pacor, S.; Mergaert, P.; Scocchi, M.; Wilson, D. N. fragments of the nonlytic proline-rich antimicrobial peptide Bac5 kill Escherichia coli cells by inhibiting protein synthesis. *Antimicrob. Agents Chemother.* **2018**, *62*, No. e00534.

(16) Mardirossian, M.; Pérébaskine, N.; Benincasa, M.; Gambato, S.; Hofmann, S.; Huter, P.; Müller, C.; Hilpert, K.; Innis, C. A.; Tossi, A.; Wilson, D. N. The dolphin proline-rich antimicrobial peptide Tur1A

inhibits protein synthesis by targeting the bacterial ribosome. *Cell Chem. Biol.* **2018**, *25*, 530−539.
(17) Florin, T.; Maracci, C.; Graf, M.; Karki, P.; Klepacki, D.; Berninghausen, O.; Beckmann, R.; Vázquez-Laslop, N.; Wilson, D. N.; Rodnina, M. V.; Mankin, A. S. An antimicrobial peptide that inhibits translation by trapping release factors on the ribosome. *Nat. Struct. Mol. Biol.* **2017**, *24*, 752−757.
(18) Matsumoto, K.; Yamazaki, K.; Kawakami, S.; Miyoshi, D.; Ooi, T.; Hashimoto, S.; Taguchi, S. In vivo target exploration of apidaecin based on Acquired Resistance induced by Gene Overexpression (ARGO assay). *Sci. Rep.* **2017**, *7*, 12136.
(19) Bluhm, M. E. C.; Knappe, D.; Hoffmann, R. Structure-activity relationship study using peptide arrays to optimize Api137 for an increased antimicrobial activity against Pseudomonas aeruginosa. *Eur. J. Med. Chem.* **2015**, *103*, 574−582.
(20) Knappe, D.; Ruden, S.; Langanke, S.; Tikkoo, T.; Ritzer, J.; Mikut, R.; Martin, L. L.; Hoffmann, R.; Hilpert, K. Optimization of oncocin for antibacterial activity using a SPOT synthesis approach: extending the pathogen spectrum to Staphylococcus aureus. *Amino Acids* **2016**, *48*, 269−280.
(21) Guida, F.; Benincasa, M.; Zahariev, S.; Scocchi, M.; Berti, F.; Gennaro, R.; Tossi, A. Effect of size and N-terminal residue characteristics on bacterial cell penetration and antibacterial activity of the proline-rich peptide Bac7. *J. Med. Chem.* **2015**, *58*, 1195−1204.
(22) Mardirossian, M.; Sola, R.; Beckert, B.; Collis, D. W. P.; Di Stasi, A.; Armas, F.; Hilpert, K.; Wilson, D. N.; Scocchi, M. Proline-rich peptides with improved antimicrobial activity against E. coli, K. Pneumoniae, and A. Baumannii. *ChemMedChem* **2019**, *14*, 2025−2033.
(23) Mardirossian, M.; Sola, R.; Degasperi, M.; Scocchi, M. Search for shorter portions of the proline-rich antimicrobial peptide fragment Bac5(1-25) that retain antimicrobial activity by blocking protein synthesis. *ChemMedChem* **2019**, *14*, 343−348.
(24) Knappe, D.; Stegemann, C.; Nimptsch, A.; Kolobov, A. J., Jr.; Korableva, E.; Shamova, O.; Kokryakov, V. N.; Hoffmann, R. Chemical modifications of short antimicrobial peptides from insects and vertebrates to fight multi-drug resistant bacteria. *Adv. Exp. Med. Biol.* **2009**, *611*, 395−396.
(25) Lopez-Perez, P. M.; Grimsey, E.; Bourne, L.; Mikut, R.; Hilpert, K. Screening and optimizing antimicrobial peptides by using SPOT-Synthesis. *Front. Chem.* **2017**, *5*, 25.
(26) Lai, P.-K.; Geldart, K.; Ritter, S.; Kaznessis, Y. N.; Hackel, B. J. Systematic mutagenesis of oncocin reveals enhanced activity and insights into the mechanisms of antimicrobial activity. *Mol. Syst. Des. Eng.* **2018**, *3*, 930−941.
(27) Benincasa, M.; Scocchi, M.; Podda, E.; Skerlavaj, B.; Dolzani, L.; Gennaro, R. Antimicrobial activity of Bac7 fragments against drug-resistant clinical isolates. *Peptides* **2004**, *25*, 2055−2061.
(28) Lai, P. K.; Tresnak, D. T.; Hackel, B. J. Identification and elucidation of proline-rich antimicrobial peptides with enhanced potency and delivery. *Biotechnol. Bioeng.* **2019**, *116*, 2439−2450.
(29) Casalino, L.; Palermo, G.; Abdurakhmonova, N.; Rothlisberger, U.; Magistrato, A. Development of site-specific Mg(2+)-RNA force field parameters: a dream or reality? Guidelines from combined molecular dynamics and quantum mechanics simulations. *J. Chem. Theory Comput.* **2017**, *13*, 340−352.
(30) Casalino, L.; Palermo, G.; Rothlisberger, U.; Magistrato, A. Who activates the nucleophile in ribozyme catalysis? An answer from the splicing mechanism of group II introns. *J. Am. Chem. Soc.* **2016**, *138*, 10374−10377.
(31) Lee, M.-T.; Sun, T.-L.; Hung, W.-C.; Huang, H. W. Process of inducing pores in membranes by melittin. *Proc. Natl. Acad. Sci. U.S.A.* **2013**, *110*, 14243−14248.
(32) Kragol, G.; Hoffmann, R.; Chattergoon, M. A.; Lovas, S.; Cudic, M.; Bulet, P.; Condie, B. A.; Rosengren, K. J.; Montaner, L. J.; Otvos, L., Jr. Identification of crucial residues for the antibacterial activity of the proline-rich peptide, pyrrhocoricin. *Eur. J. Biochem.* **2002**, *269*, 4226−4237.
(33) Knappe, D.; Zahn, M.; Sauer, U.; Schiffer, G.; Sträter, N.; Hoffmann, R. Rational design of oncocin derivatives with superior protease stabilities and antibacterial activities based on the high-resolution structure of the oncocin-DnaK complex. *Chembiochem* **2011**, *12*, 874−876.
(34) Narayanan, S.; Modak, J. K.; Ryan, C. S.; Garcia-Bustos, J.; Davies, J. K.; Roujeinikova, A. Mechanism of Escherichia coli resistance to pyrrhocoricin. *Antimicrob. Agents Chemother.* **2014**, *58*, 2754−2762.
(35) Brunetti, J.; Falciani, C.; Roscia, G.; Pollini, S.; Bindi, S.; Scali, S.; Arrieta, U. C.; Gomez-Vallejo, V.; Quercini, L.; Ibba, E.; Prato, M.; Rossolini, G. M.; Llop, J.; Bracci, L.; Pini, A. In vitro and in vivo efficacy, toxicity, bio-distribution and resistance selection of a novel antibacterial drug candidate. *Sci. Rep.* **2016**, *6*, 26077.
(36) Runti, G.; Benincasa, M.; Giuffrida, G.; Devescovi, G.; Venturi, V.; Gennaro, R.; Scocchi, M. The mechanism of killing by the proline-rich peptide Bac7(1-35) against clinical strains of Pseudomonas aeruginosa differs from that against other gram-negative bacteria. *Antimicrob. Agents Chemother.* **2017**, *61*, No. e01660.
(37) Moncla, B. J.; Pryke, K.; Rohan, L. C.; Graebing, P. W. Degradation of naturally occurring and engineered antimicrobial peptides by proteases. *Adv. Biosci. Biotechnol.* **2011**, *2*, 404−408.
(38) Mattiuzzo, M.; Gobba, C. D.; Runti, G.; Mardirossian, M.; Bandiera, A.; Gennaro, R.; Scocchi, M. Proteolytic activity of Escherichia coli oligopeptidase B against proline-rich antimicrobial peptides. *J. Microbiol. Biotechnol.* **2014**, *24*, 160−167.
(39) Mardirossian, M.; Pompilio, A.; Crocetta, V.; De Nicola, S.; Guida, F.; Degasperi, M.; Gennaro, R.; Di Bonaventura, G.; Scocchi, M. In vitro and in vivo evaluation of BMAP-derived peptides for the treatment of cystic fibrosis-related pulmonary infections. *Amino Acids* **2016**, *48*, 2253−2260.
(40) Hilpert, K.; Winkler, D. F.; Hancock, R. E. Peptide arrays on cellulose support: SPOT synthesis, a time and cost efficient method for synthesis of large numbers of peptides in a parallel and addressable fashion. *Nat. Protoc.* **2007**, *2*, 1333−1349.
(41) Kuipers, B. J. H.; Gruppen, H. Prediction of molar extinction coefficients of proteins and peptides using UV absorption of the constituent amino acids at 214 nm to enable quantitative reverse phase high-performance liquid chromatography-mass spectrometry analysis. *J. Agric. Food Chem.* **2007**, *55*, 5445−5451.
(42) Baba, T.; Ara, T.; Hasegawa, M.; Takai, Y.; Okumura, Y.; Baba, M.; Datsenko, K. A.; Tomita, M.; Wanner, B. L.; Mori, H. Construction of Escherichia coli K-12 in-frame, single-gene knockout mutants: the Keio collection. *Mol. Syst. Biol.* **2006**, *2*, 2006.0008.
(43) Leoni, G.; De Poli, A.; Mardirossian, M.; Gambato, S.; Florian, F.; Venier, P.; Wilson, D.; Tossi, A.; Pallavicini, A.; Gerdol, M. Myticalins: A novel multigenic family of linear, cationic antimicrobial peptides from Marine Mussels (Mytilus spp.). *Mar. Drugs* **2017**, *15*, 261.
(44) Polikanov, Y. S.; Melnikov, S. V.; Söll, D.; Steitz, T. A. Structural insights into the role of rRNA modifications in protein synthesis and ribosome assembly. *Nat. Struct. Mol. Biol.* **2015**, *22*, 342−344.
(45) Kabsch, W. Xds. *Acta Crystallogr., Sect. D: Biol. Crystallogr.* **2010**, *66*, 125−132.
(46) McCoy, A. J.; Grosse-Kunstleve, R. W.; Adams, P. D.; Winn, M. D.; Storoni, L. C.; Read, R. J. Phasercrystallographic software. *J. Appl. Crystallogr.* **2007**, *40*, 658−674.
(47) Adams, P. D.; Afonine, P. V.; Bunkóczi, G.; Chen, V. B.; Davis, I. W.; Echols, N.; Headd, J. J.; Hung, L.-W.; Kapral, G. J.; Grosse-Kunstleve, R. W.; McCoy, A. J.; Moriarty, N. W.; Oeffner, R.; Read, R. J.; Richardson, D. C.; Richardson, J. S.; Terwilliger, T. C.; Zwart, P. H. PHENIX: a comprehensive Python-based system for macromolecular structure solution. *Acta Crystallogr., Sect. D: Biol. Crystallogr.* **2010**, *66*, 213−221.
(48) Emsley, P.; Cowtan, K. Coot: model-building tools for molecular graphics. *Acta Crystallogr., Sect. D: Biol. Crystallogr.* **2004**, *60*, 2126−2132.

(49) Case, D. A.; Darden, T.; Cheatham, T. E.; Simmerling, C.; Wang, J.; Duke, R. E.; Luo, R.; Walker, R. C.; Zhang, W.; Merz, K. M. *AMBER 2016*; University of California: San Francisco, 2016.
(50) Van Der Spoel, D.; Lindahl, E.; Hess, B.; Groenhof, G.; Mark, A. E.; Berendsen, H. J. C. GROMACS: fast, flexible, and free. *J. Comput. Chem.* **2005**, *26*, 701−718.
(51) Maier, J. A.; Martinez, C.; Kasavajhala, K.; Wickstrom, L.; Hauser, K. E.; Simmerling, C. ff14SB: improving the accuracy of protein side chain and backbone parameters from ff99SB. *J. Chem. Theory Comput.* **2015**, *11*, 3696−3713.
(52) Pérez, A.; Marchán, I.; Svozil, D.; Sponer, J.; Cheatham, T. E., 3rd; Laughton, C. A.; Orozco, M. Refinement of the AMBER Force Field for Nucleic Acids: Improving the Description of α/γ Conformers. *Biophys. J.* **2007**, *92*, 3817−3829.
(53) Aduri, R.; Psciuk, B. T.; Saro, P.; Taniga, H.; Schlegel, H. B.; SantaLucia, J. AMBER force field parameters for the naturally occurring modified nucleosides in RNA. *J. Chem. Theory Comput.* **2007**, *3*, 1464−1475.
(54) Šponer, J.; Krepl, M.; Banáš, P.; Kührová, P.; Zgarbová, M.; Jurečka, P.; Havrila, M.; Otyepka, M. How to understand atomistic molecular dynamics simulations of RNA and protein-RNA complexes? *Wiley Interdiscip. Rev.: RNA* **2017**, *2*, No. e1405.
(55) Åqvist, J. Ion water interaction potentials derived from free-energy perturbation simulations. *J. Phys. Chem.* **1990**, *94*, 8021−8024.
(56) Joung, I. S.; Cheatham, T. E. Determination of alkali and halide monovalent ion parameters for use in explicitly solvated biomolecular simulations. *J. Phys. Chem. B* **2008**, *112*, 9020−9041.
(57) Pang, Y.-P. Novel zinc protein molecular dynamics simulations: Steps toward antiangiogenesis for cancer treatment. *J. Mol. Model.* **1999**, *5*, 196−202.
(58) Jorgensen, W. L.; Chandrasekhar, J.; Madura, J. D.; Impey, R. W.; Klein, M. L. Comparison of simple potential functions for simulating liquid water. *J. Chem. Phys.* **1983**, *79*, 926−935.
(59) Sousa da Silva, A. W.; Vranken, W. F. ACPYPE - AnteChamber PYthon Parser interfacE. *BMC Res. Notes* **2012**, *5*, 367.
(60) Casalino, L.; Palermo, G.; Spinello, A.; Rothlisberger, U.; Magistrato, A. All-atom simulations disentangle the functional dynamics underlying gene maturation in the intron lariat spliceosome. *Proc. Natl. Acad. Sci. U.S.A.* **2018**, *115*, 6584−6589.
(61) Berendsen, H. J. C.; Postma, J. P. M.; van Gunsteren, W. F.; Di Nola, A.; Haak, J. R. Molecular-Dynamics with Coupling to an External Bath. *J. Chem. Phys.* **1984**, *81*, 3684−3690.
(62) Bussi, G.; Donadio, D.; Parrinello, M. Canonical sampling through velocity rescaling. *J. Chem. Phys.* **2007**, *126*, 014101.
(63) Parrinello, M.; Rahman, A. Crystal-structure and pair potentials - a molecular-dynamics study. *Phys. Rev. Lett.* **1980**, *45*, 1196−1199.
(64) Parrinello, M.; Rahman, A. Polymorphic transitions in single crystals: A new molecular dynamics method. *J. Appl. Physiol.* **1981**, *52*, 7182−7190.
(65) Hess, B.; Bekker, H.; Berendsen, H. J. C.; Fraaije, J. G. E. M. LINCS: A linear constraint solver for molecular simulations. *J. Comput. Chem.* **1997**, *18*, 1463−1472.
(66) Darden, T.; York, D.; Pedersen, L. Particle mesh Ewald: An N·log(N) method for Ewald sums in large systems. *J. Chem. Phys.* **1993**, *98*, 10089−10092.
(67) Humphrey, W.; Dalke, A.; Schulten, K. VMD: Visual molecular dynamics. *J. Mol. Graphics* **1996**, *14*, 33−38.